

Observation of a quenched moment of inertia in a rotating strongly interacting Fermi gas

Bason Clancy, Le Luo, and John E. Thomas*

Duke University, Department of Physics, Durham, North Carolina, 27708, USA

(Dated: August 24, 2021)

We make a model-independent measurement of the moment of inertia of a rotating, expanding strongly-interacting Fermi gas. Quenching of the moment of inertia is observed for energies both below and above the superfluid transition. This shows that a strongly interacting Fermi gas with angular momentum can support irrotational flow in both the superfluid and collisional normal fluid regimes.

Strongly interacting Fermi gases [1] provide a unique paradigm for exploring strongly interacting nearly perfect fluids in nature, from high temperature superfluids and superconductors to exotic normal fluids, such as the quark-gluon plasma of the Big Bang [2, 3], or low viscosity quantum fields [4]. Rotating superfluids require irrotational flow, which quenches the moment of inertia or produces a vortex lattice [5]. Recently, the observation of vortices has directly demonstrated superfluidity in a strongly interacting Fermi gas [6]. However, the moment of inertia has not been measured and the rotational properties have not been characterized in the normal regime, where irrotational flow is not required.

We report a measurement of the moment of inertia I of a strongly interacting Fermi gas of ${}^6\text{Li}$ atoms in both the superfluid and normal fluid regimes, by releasing rotating clouds from a cigar-shaped optical trap. In the superfluid regime, a rapid increase in the angular velocity is observed as the cloud expands, indicating a quenching of I to values as low as 0.05 of the rigid body value. However, quenching persists for energies far above the superfluid transition, in contrast to previous measurements spanning half a century, in nuclei [7, 8], liquid helium [9] and Bose-Einstein condensates (BEC's) [10, 11], where irrotational behavior was attributed only to superfluidity. Our results demonstrate that a strongly interacting Fermi gas with angular momentum can support irrotational flow not only in the superfluid regime, but also in the normal fluid regime, which we attribute to nearly perfect collisional hydrodynamics.

Strongly interacting Fermi gases exhibit hydrodynamic behavior in both the superfluid and normal fluid regimes. While superfluidity explains the low temperature hydrodynamics [12], the origin of nearly ideal flow in the normal fluid remains an open question [13]. The hydrodynamics of the gas has been studied in expansion dynamics [1, 14, 15, 16], and in collective modes [12, 17, 18, 19], but is also predicted to dramatically affect the rotational properties [20], which have been investigated only in vortices [6, 16]. Vortices demonstrate irrotational hydrodynamic flow, but only form at temperatures well below the superfluid transition [6]. In contrast, measurement of the moment of inertia provides a probe of the rotational

properties in both the normal and superfluid regimes.

In our experiments, a strongly interacting Fermi gas is prepared using a 50:50 mixture of the two lowest hyperfine states of ${}^6\text{Li}$ atoms in an ultrastable CO_2 laser trap with a bias magnetic field tuned to a broad Feshbach resonance at $B = 834$ G [21]. At 834 G, the gas is cooled to quantum degeneracy through forced evaporation by lowering the trap depth U [1]. Then U is recompressed to $U_0/k_B = 100$ μK , which is large compared to the energy per particle of the gas.

At the final trap depth U_0 , the measured oscillation frequencies in the transverse directions are $\omega_x = 2\pi \times 2354(4)$ Hz and $\omega_y = 2\pi \times 1992(2)$ Hz, while the axial frequency is $\omega_z = 2\pi \times 71.1(3)$ Hz, producing a cigar-shaped trap with $\lambda = \omega_z/\omega_x = 0.030$. The total number of atoms at is typically $N = 1.3 \times 10^5$. The corresponding Fermi energy E_F and Fermi temperature T_F for an ideal (noninteracting) harmonically trapped gas at the trap center are $E_F = k_B T_F = \hbar \bar{\omega} (3N)^{1/3}$, where $\bar{\omega} = (\omega_x \omega_y \omega_z)^{1/3}$. For our trap conditions, $T_F = 2.4$ μK .

After evaporation and recompression, we typically achieve energies of $E = 0.56 E_F$, which is close to the ground state energy of $E = 0.50 E_F$ [22]. To heat the sample, energy is added by releasing and then recapturing the gas, after which the gas is allowed to reach equilibrium for 0.5 s. The total energy E of the cloud is determined in the universal, strongly interacting regime from the mean square axial (z) cloud size, using $E = 3m\omega_z^2 \langle z^2 \rangle$, where m is the atom mass [22, 23].

Once the gas has been prepared in the desired energy state, it is rotated by suddenly changing the direction of CO_2 laser beam as shown in Fig. 1. Rotation of the cigar-shaped CO_2 laser trap is accomplished by changing the frequency of the acousto-optic modulator (AOM) that controls the trap laser intensity, using a radiofrequency (rf) switch. When the frequency is changed, the direction of the trapping laser beam changes, causing the position of the beam on the final focusing lens to translate. This translation causes primarily a rotation of the cigar-shaped trap at the focal point, about an axis (y) perpendicular to the plane of the cigar-shaped trap. A scissors mode [24] is excited by the rotation. Then the cloud is permitted to oscillate in the trap for a chosen

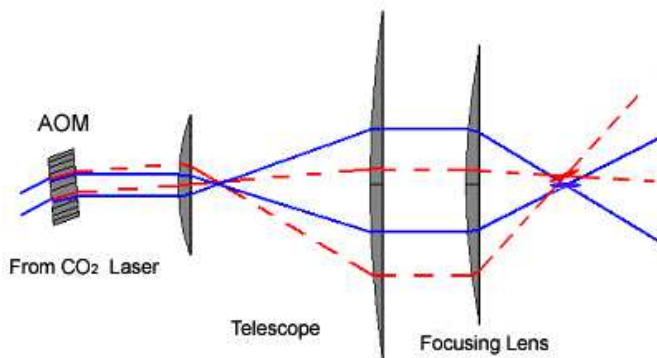


FIG. 1: Scheme to rotate the optical trap. The optical trap is rotated by changing the frequency of an acousto-optic modulator (AOM). The rotation adds angular momentum to the trapped cloud before release.

period that determines the initial angular velocity of the cloud before release.

Fig. 2 shows cloud images as a function of expansion time for the coldest samples, with a typical energy $E = 0.56E_F$ near the ground state. When the gas is released without rotation of the trap, Fig. 2 (top), the Fermi cloud expands anisotropically, as previously predicted [25] and observed [1, 14]. In that case, the gas expands rapidly in the narrow (x,y) directions of the cigar, while remaining nearly stationary in the long (z) direction, inverting the aspect ratio σ_x/σ_z as the cloud becomes elliptical in shape.

Quite different expansion dynamics occurs when the cloud is rotating prior to release, Fig. 2 (middle) and (bottom), which demonstrates irrotational flow in a nearly perfect hydrodynamic regime. In this case, the aspect ratio σ_x/σ_z initially increases toward unity. However, as the aspect ratio approaches unity, the moment of inertia decreases and the angular velocity of the principal axes increases to conserve angular momentum as previously predicted [26] and observed [10, 11] in a superfluid BEC. After the aspect ratio reaches a maximum less than unity [26], it and the angular velocity begin to decrease as the angle of the cigar shaped cloud approaches a maximum value less than 90° .

Fig. 3 shows the measured aspect ratio and the angle of the principal axes versus expansion time, which are determined from the cloud images. The measured density profiles are fit with a two-dimensional gaussian distribution, which takes the form $A \exp[-az^2 - bzx - cx^2]$. From the values of a, b, and c, the aspect ratio of the rotated cloud and the angle of the long axis of the cloud with respect to the laboratory z-axis are determined.

We attempt to model the data for measurements near the ground state (blue solid circles and green triangles of Fig. 3), by using a zero temperature hydrodynamic theory for the expansion of a rotating strongly-interacting Fermi gas in the superfluid regime. A theory of this type

was first used to describe the rotation and expansion of a weakly interacting BEC [26, 27]. The model consists of the Euler and continuity equations for a superfluid, where the velocity field \mathbf{v} is irrotational, i.e., $\nabla \times \mathbf{v} = 0$. The driving force for the expansion arises from the gradient of the chemical potential, which we take to be that of a strongly interacting Fermi gas [1, 20]. We also include the force arising from magnet field curvature, which changes the angular momentum at the point of maximum aspect ratio by 10% and the angle and aspect ratio at the longest release times by a few percent. To determine the initial conditions for our model, we directly measure the initial angular velocity and axial cloud radius just after release, while assuming the transverse radii are given by zero temperature values for our trap frequencies. The results yield excellent agreement with all of the Fermi gas angle and aspect ratio data, with no free parameters, as shown in Fig. 3.

We make a model-independent measurement of the effective moment of inertia $I \equiv L/\Omega$, where Ω is the angular velocity of the principal axes of the cloud after release and $L = \Omega_0 I_0$ is the angular momentum, which is conserved during the expansion (we neglect the small change arising from the magnetic potential). The angular velocity Ω is calculated from the time derivative of a polynomial fit to the angle versus time data. To determine the initial moment of inertia I_0 , we note that for a cigar-shaped cloud with a small aspect ratio σ_x/σ_z , the moment of inertia for the irrotational fluid is nearly equal to the rigid body value [11, 26]. For our parameters $I_0 \simeq Nm\langle z^2 \rangle_0$, within 0.3% accuracy, where $\langle z^2 \rangle_0$ is measured with respect to the principal axes of the cloud. Correspondingly, the initial angular momentum of the cloud is essentially equal to the rigid body value just after release. The measured effective moment of inertia after release is then $I = I_0 \Omega_0/\Omega$. The corresponding rigid body moment of inertia is determined from the fit to the cloud profile, $I_{rig} = Nm\langle x^2 + z^2 \rangle$. Hence, we obtain $I/I_{rig} = (\Omega_0/\Omega)I_0/I_{rig}$.

Fig. 4 shows the measured minimum value of I/I_{rig} as a function of initial angular velocity Ω_0 . The smallest values of I/I_{rig} occur for the smallest Ω_0 . For the coldest clouds (blue solid circles), where the energy of the gas is close to that of the ground state, the gas is believed to be in the superfluid regime [6, 12, 22]. In this case, we observe values of I/I_{rig} as small as 0.05, smaller than those obtained from the scissors mode of a BEC of atoms [28, 29]. The solid line shows I/I_{rig} as predicted by the superfluid hydrodynamic theory, which is in very good agreement with the measurements.

Such nearly perfect irrotational flow usually arises only in the superfluid regime. For example, normal weakly interacting Bose gases expand ballistically above the critical temperature. We observe ballistic expansion of the Fermi gas at 528 G, where the scattering length vanishes. In this case, after release of the rotating cloud, there is

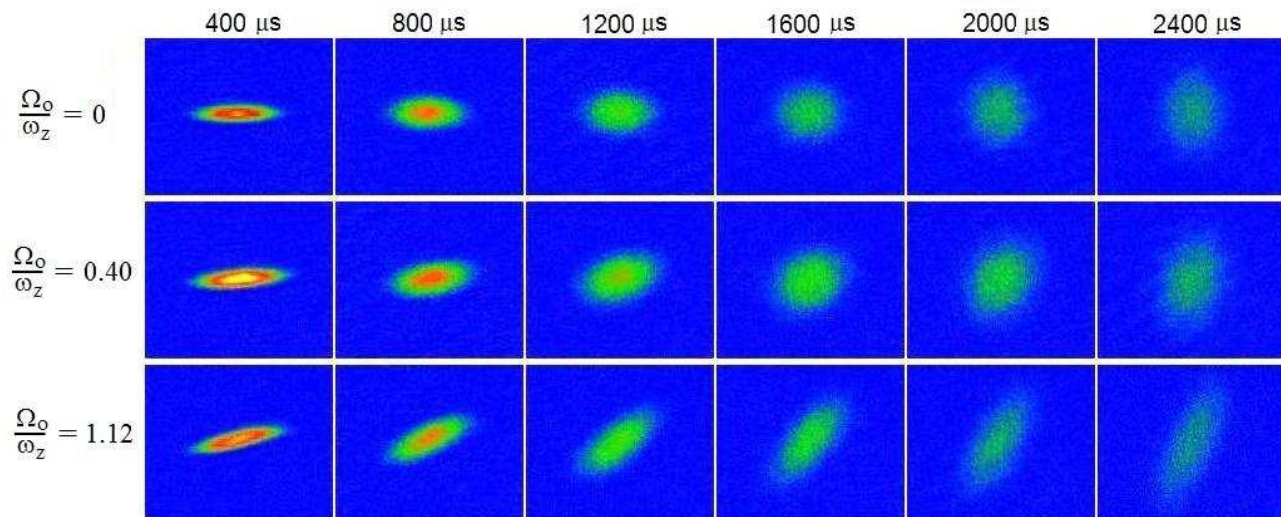


FIG. 2: Expansion of a rotating, strongly interacting Fermi gas. The initial angular velocity Ω_0 is given in units of the trap axial frequency ω_z .

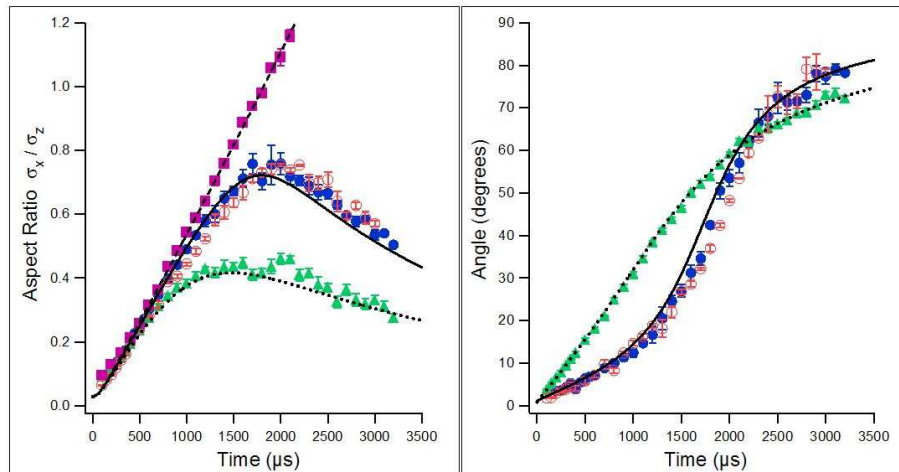


FIG. 3: Aspect ratio and angle of the principal axis versus time. Purple squares (no angular velocity); Blue solid circles ($\Omega_0/\omega_z = 0.40$, $E/E_F = 0.56$); Red open circles ($\Omega_0/\omega_z = 0.40$, $E/E_F = 2.1$); Green triangles ($\Omega_0/\omega_z = 1.12$, $E/E_F = 0.56$). The solid, dashed, and dotted lines are the theoretical calculations using the measured initial conditions.

no evidence of irrotational hydrodynamics. The aspect ratio asymptotically approaches unity, and there is no increase in angular velocity.

In contrast, for a normal strongly interacting Fermi gas, we observe quenching of the moment of inertia. To investigate the normal fluid regime, we increase E above the transition energy, which we estimate to be $E_c = 0.94 E_F$ [22]. The open red circles in Fig. 3, show the aspect ratio and angle versus time for $E = 2.1 E_F$ and an initial angular velocity $\Omega_0/\omega_z = 0.4$. The results are nearly identical to those obtained for $\Omega_0/\omega_z = 0.4$ in the superfluid regime (blue solid circles). We attribute this result to nearly perfect collisional hydrodynamics in the normal strongly interacting fluid, although a com-

plete many-body microscopic description of this regime does not yet exist.

We see from Fig. 4 that the moment of inertia is quenched for energies both above and below the superfluid transition. Irrotational hydrodynamics generally requires the quenched moment of inertia to be given by [26]

$$I/I_{rig} = \delta^2 \equiv \langle z^2 - x^2 \rangle^2 / \langle z^2 + x^2 \rangle^2, \quad (1)$$

where δ^2 is computed with respect to the principal axes. Fig. 5 compares the measured minimum values of I/I_{rigid} with the values of δ^2 obtained from the measured cloud aspect ratios, which directly verifies this prediction.

We have observed quenching of the moment of inertia of a strongly interacting Fermi gas over a wide range of

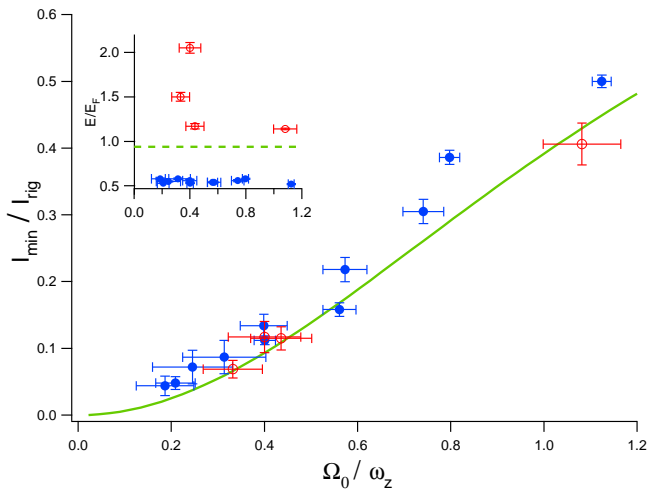


FIG. 4: Quenching of the moment of inertia versus initial angular velocity Ω_0 . I_{min} is the minimum moment of inertia measured during expansion. I_{rig} is the rigid body moment of inertia corresponding to the cloud profile. Blue solid circles- initial energy before rotation below the superfluid transition energy $E_c = 0.94 E_F$. Red open circles- initial energy before rotation above the superfluid transition energy. Insert shows the energy for each data point. The dashed line shows the superfluid transition energy E_c .

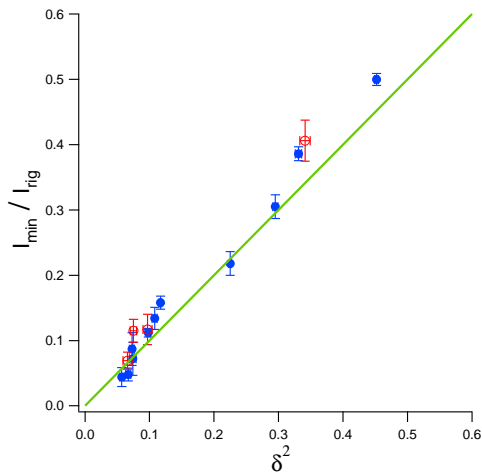


FIG. 5: Quenching of the moment of inertia versus the measured cloud deformation factor δ^2 . Blue solid circles- initial energy before rotation below the superfluid transition energy $E_c = 0.94 E_F$. Red open circles - initial energy before rotation above the superfluid transition energy.

energies, demonstrating nearly perfect irrotational flow and low viscosity hydrodynamics in both the superfluid and normal regimes. Our observations show that these properties, which have been suggested as signatures of superfluidity in the past [30], also appear in the normal strongly interacting fluid. These results have important implications for other strongly interacting systems in nature. It is known that quark-gluon plasmas, as created

recently in heavy ion accelerators, exhibit minimum viscosity hydrodynamics and elliptic flow [2, 3]. It is therefore possible that irrotational flow will alter the signature of quark-gluon plasmas with finite angular momentum.

This research was supported by the Chemical Sciences, Geosciences and Biosciences Division of the Office of Basic Energy Sciences, Office of Science, U. S. Department of Energy, the Physics Divisions of the Army Research Office and the National Science Foundation.

* jet@phy.duke.edu

- [1] K. M. O'Hara, et al., *Science* **298**, 2179 (2002).
- [2] P. F. Kolb and U. Heinz, *Quark Gluon Plasma 3* (World Scientific, 2003), p. 634.
- [3] E. Shuryak, *Prog. Part. Nucl. Phys.* **53**, 273 (2004).
- [4] P.K.Kovtun, D.T.Son, and A.O.Starinets, *Phys. Rev. Lett.* **94**, 111601 (2005).
- [5] F. London, *Superfluids* (John Wiley and Sons, New York, 1954), vol. 2, p. 144.
- [6] M. Zwierlein, et al., *Nature* **435**, 1047 (2005).
- [7] A. B. Migdal, *Nucl. Phys.* **13**, 655 (1959).
- [8] K.Alder, et al., *Rev. Mod. Phys.* **28**, 432 (1956).
- [9] G.B.Hess and W.M.Fairbank, *Phys. Rev. Lett.* **19**, 216 (1967).
- [10] G.Hechenblaikner, et al., *Phys. Rev. Lett.* **19**, 216 (1967).
- [11] M. Modugno, et al., *Phys. Rev. A* **67**, 023608 (2003).
- [12] J. Kinast, et al., *Phys. Rev. Lett.* **92**, 150402 (2004).
- [13] P. Massignan, G. M. Bruun, and H. Smith, *Phys. Rev. A* **71**, 033607 (2005).
- [14] T. Bourdel, et al., *Phys. Rev. Lett.* **91**, 020402 (2003).
- [15] C. A. Regal and D. S. Jin, *Phys. Rev. Lett.* **90**, 230404 (2003).
- [16] C. H. Schunck, et al., *Phys. Rev. Lett.* **98**, 050404 (2007).
- [17] J. Kinast, A. Turlapov, and J. E. Thomas, *Phys. Rev. Lett.* **94**, 170404 (2005).
- [18] M. Bartenstein, et al., *Phys. Rev. Lett.* **92**, 203201 (2004).
- [19] A. Altmeyer, et al., *Phys. Rev. Lett.* **98**, 040401 (2007).
- [20] M. Cozzini and S. Stringari, *Phys. Rev. Lett.* **91**, 070401 (2003).
- [21] M. Bartenstein, et al., *Phys. Rev. Lett.* **94**, 103201 (2005).
- [22] L. Luo, et al., *Phys. Rev. Lett.* **98**, 080402 (2007).
- [23] J. E. Thomas, A. Turlapov, and J. Kinast, *Phys. Rev. Lett.* **95**, 120402 (2005).
- [24] Guéry-Odelin and S. Stringari, *Phys. Rev. Lett.* **83**, 4452 (1999).
- [25] C. Menotti, P. Pedri, and S. Stringari, *Phys. Rev. Lett.* **89**, 250402 (2002).
- [26] M. Edwards, et al., *Phys. Rev. Lett.* **88**, 070405 (2002).
- [27] A.Recati, F.Zambelli, and S. Stringari, *Phys. Rev. Lett.* **86**, 377 (2001).
- [28] F.Zambelli and S. Stringari, *Phys. Rev. A* **63**, 033602 (2001).
- [29] O.M.Maragó, et al., *J. Phys.: Condens Matter* **14**, 343 (2002).
- [30] K. Huang, in *Bose-Einstein Condensation*, edited by A.Griffin, D.W.Snoke, and S.Stringgari (Cambridge University Press, 1995), p. 31.